Modeling and Analysis of Resonant Switched Capacitor Converters with Free-Wheeling ZCS

Eli Hamo, Michael Evzelman, and Mor Mordechai Peretz
Power Electronics Laboratory
Department of Electrical and Computer Engineering
Ben-Gurion University of the Negev
P.O. Box 653, Beer-Sheva, 84105 Israel
eliham@bgu.ac.il ; evzelman@ee.bgu.ac.il ; morp@ee.bgu.ac.il
Website: www.ee.bgu.ac.il/~pel/

***Abstract*—This paper introduces a unified modeling methodology to describe and explore the loss mechanism of resonant Switched Capacitor Converter (SCC) operating in a self-commutation zero current switching. The conventional equivalent resistance concept, which assumes a single conduction path of the resonant current, is generalized to model the losses in cases where the resonant current is divided across several conduction loops. The new modeling concept is compatible to describe the losses resulting from resistive elements as well as P-N junction devices, offering a closed-form solution for the equivalent resistance. Verification of the concept has been carried out by simulations and experiments on 3 – 30W unity and double gain resonant SCC with free-wheeling ZCS. A very good agreement is obtained between the theoretical calculations, simulations and experimental results, well demonstrating the model capability to identify the loss contributors in each conduction path.**

I. Introduction

In Resonant Switched Capacitor Converters (RSCC) operation, Zero Current Switching (ZCS) is mandatory to achieve high power conversion efficiency and reliability. ZCS can be achieved by employing an active monitoring and control of the resonant current [1], [2]. This requires complex control scheme and circuitry. Alternatively, ZCS can be obtained by unidirectional switches, e.g. inserting a diode in series to the active switch. In this case, ZCS is assured by simple means at the cost of increased conduction losses. To overcome the deficiencies of these methods, a simple and efficient self-commutation concept as illustrated in Fig. 1 has been presented in [3]-[5]. It consists of a transistor that conducts for the majority of the resonant cycle, and a parallel diode that acts as a free-wheeling element such that turn off occurs at zero current. This method exhibits both advantages of inherent ZCS and overcomes the deficiencies of previous methods such as high conduction losses and complex control hardware. However, due to a Divided Conduction Path (DCP) of the resonant current (Fig. 1), the conventional equivalent resistance analysis to evaluate the losses [6]-[9], cannot directly be applied in this case.

The objective of this paper is to describe and explore the loss mechanism of resonant SCC operating in a self-commutation ZCS mode.

The new modeling methodology extends the modeling concept employed in [6]-[12], to take into account the DCP of a single charge/discharge state.

The deliverables of this modeling approach are on both theoretical and practical realms, it provides a streamlined procedure to design a reliable and low-cost soft-switched SCC, as well as an insight into the dominant contributors of losses in DCP operation mode.

II. Basic Terminology and Definitions

Throughout the paper, the modeling concept will be explained on a unity gain resonant SCC (Fig. 2). Even though the exemplary circuit is not the best candidate to showcase the strength of ZCS, it highlights the mechanism of DCP operation and is therefore selected.

Resonant SCC that operates in open-loop can be represented by an equivalent circuit, [13]-[19], which consists of a target voltage source, V_T, that represents the no load output voltage of the converter, and a series equivalent resistance, R_e, that stands for the conduction losses caused by the current flow in the series resistances of the capacitor's charge/discharge path.

Self-commutated unity gain SCC (Fig. 2) operates in two phases. The charging phase is split into two sub-states, as marked in timing diagram (Fig. 1). First, the switch S_1 is turned on, and the capacitor C_f is charged resonantly. Next, approaching the end of half resonant cycle, S_1 is turned off, and the free-wheeling diode conducts until the current reaches zero. The second phase starts by turning S_2 on, and C_f resonantly discharges onto the output.

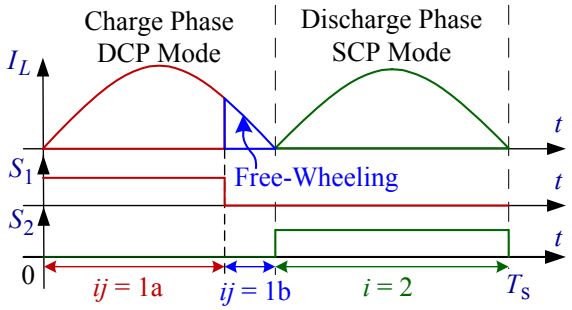

Fig. 1. Typical resonant current waveforms during a: Charge phase - DCP operation, Discharge phase – SCP operation.

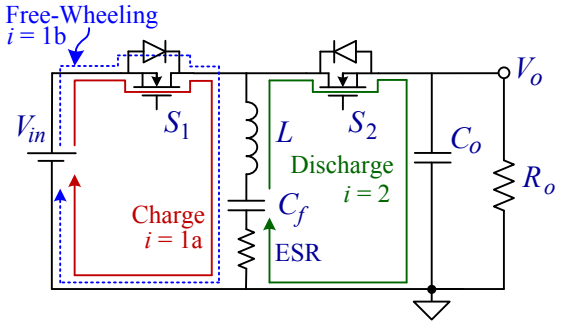

Fig. 2. Unity gain SCC with free-wheeling ZCS of the charge state.

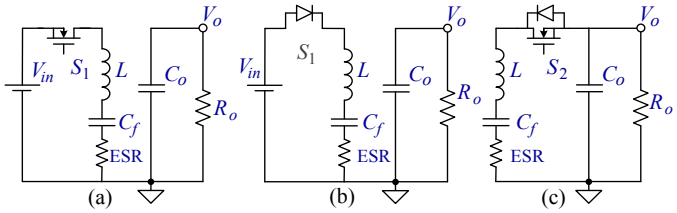

Fig. 3. Operation states of unity gain SCC (Fig. 2): (a) Charging sub-state *ij* = 1a, (b) Charging sub-state *ij* = 1b, (c) Discharging state *i* = 2.

To facilitate systematical analysis, the following definitions and terminology are used: *phase* - relates to a time period of half resonant cycle, e.g. *charging phase*, or *discharging phase* (Fig. 1), denoted by a numerical index i = 1,2 …; *sub-state* – a portion of a *phase*, denoted by an alphabetical index j = a,b …; Single Conduction Path (SCP) – a *phase* that includes one *sub-state* only; *Divided Conduction Path* (DCP) – a *phase* that includes more than one *sub-state*. For example, sub-state 'a' at phase 1 (red lines in Figs. 1, 2), will be denoted as ij = 1a.

III. Modeling Approach

The generic approach to extract the equivalent model of resonant SCC operating in the particular case of SCP has been presented in [6]-[9]. Generalization of the model to include DCP operation requires the following steps: first, based on the switching sequence applied to the SCC, each phase is described by one or more sub-states according to the operation mode (SCP or DCP). Given the example on hand, the operation of SCC in Fig. 2 is represented by three sub-circuits, that is, charging sub-state by transistor conduction (Fig. 3a), charging sub-state by free-wheeling diode (Fig. 3b), and discharge phase (Fig. 3c).

Second, each of the sub-circuits is simplified to a lumped RLC circuit as shown in Fig. 4. This circuit is used to describe the operation of each sub-circuit in it's relevant conduction time, where ΔV_i is the initial voltage difference between the charging/discharging source and the resonant tank voltage, R_{ij} is the total loop resistance (switch resistance R_{Si}, inductor resistance R_{Li} and capacitor ESR), C_i and L_i are the total capacitance and inductance of the loop, respectively.

The next step applies the calculation of the power loss, P_{ij}, due to the series resistances R_{ij} of each sub-state, and expressing it as a function of the average capacitor current I_{avi}. The average capacitor current of each phase is linearly proportional to the average output current [6], [17], [18]. By doing so, the power dissipated in each phase, is referenced to the output current, using the proportionality factor k_i. The equivalent resistances of each sub-state, R_{eij}, are then extracted from the dissipated power, P_{ij}.

The general case of DCP applies a free-wheeling mode realized by diode conduction. Since the dominant loss contributor of the diode is the average current, an additional proportionality factor is required to relate the average sub-state current to the total average current of the phase in which it exists in (Fig. 5). In this study this factor is referred as ρ_{ij}, and the relationship between the average currents can now be expressed as:

$$I_{av1a} = \rho_{1a} \cdot I_{av1};\ \ I_{av1b} = \rho_{1b} \cdot I_{av1}, \qquad (1)$$

where I_{av1} is the phase current, which equals to the sum of the average capacitor currents during each sub-state I_{av1a} plus I_{av1b}. It should be noted, that the averaging method applied here considers the contribution of the sub-state average current on the entire switching period, that is:

$$I_{avi} = \frac{q_i}{T_s};\ \ I_{avia} = \frac{q_{ia}}{T_s}, \qquad (2)$$

where q_i is the total charge of the i^{th} phase, q_{ia} is the charge of the sub-state 'a' while commutated at the angle $\varphi_i = \pi \cdot T_{ia}/T_i$ (Fig. 5). Therefore, the diode loss contribution can be represented as a function of the phase current, i.e. by a voltage source, V_{dij}, that takes into account the partial average current in the sub-state as follows:

$$V_{dij} = k_i \cdot \rho_{ij} \cdot V_{Fij}, \qquad (3)$$

where V_{Fij} is the average voltage drop across the diode due to current through it at sub-state, j, in phase, i.

Finally, the model is constructed by considering series connection of the equivalent resistances, R_{eij} and the voltage source, V_{dij}, between the target voltage and the output port. As a result, the SCC in Fig. 2 operating in DCP mode is represented by the average equivalent model circuit of Fig. 6.

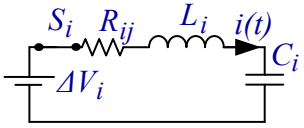

Fig. 4. The basic and generic instantaneous RLC sub-circuit.

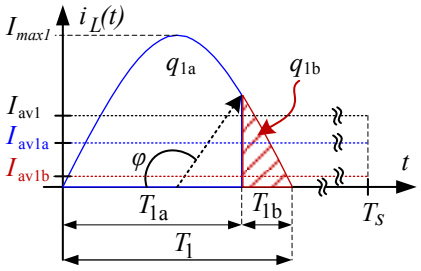

Fig. 5. DCP switching phase current waveform.

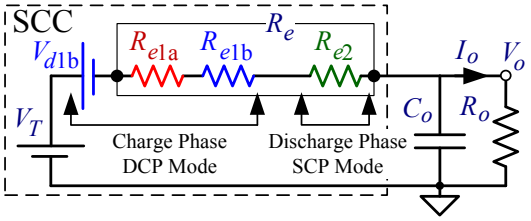

Fig. 6. SCC generic average equivalent circuit that shows the contribution of the partial sub-circuits equivalent resistances R_{ei} to the total equivalent circuit resistance R_e. For the unity gain SCC example of Fig. 2, R_{e1a} is the loss contribution of charge sub-state 1a, R_{e1b} and V_{d1b} are the resistive and diode loss contribution of the free-wheeling sub-state, respectively, R_{e2} is the loss contribution of discharging phase.

IV. Extraction of Equivalent Resistances and Equivalent Average Voltage Drop

Following the modeling methodology described earlier, the equivalent resistance value is extracted in this section. It is assumed that each RLC sub-state (Fig. 4) operates under ZCS conditions, and the quality factor, Q_{ij}, is sufficiently high (Q_{ij}>5).

As a result, the peak currents I_{pki}, I_{pkij} are considered equal. For the case of the circuit in Fig. 2, this applies the following:

$$I_{pki} = I_{pkia} = I_{pkib}, \tag{4}$$

where I_{pki} , I_{pkia}, I_{pkib}, are the potential peak currents that are, or could be developed given the conditions of the switching phase *i*, or the sub-state *j*, *i*a and *i*b, respectively.

A. Equivalent resistance calculation

The energy, E_{ia}, dissipated in the sub-circuit due to the loop resistance, R_{ia} (Fig. 4) and the current during the time interval T_{ia} (Fig. 5) is derived by integrating the instantaneous power $p(t) = i_C^2(t)\cdot R_{ia}$ ($i_C(t)$ is the capacitor current) over the sub-state time interval, T_{ia}:

$$E_{ia} = R_{ia}\cdot\left(I_{pki}\right)^2\cdot\int_0^{\varphi_i/\omega_{0ia}}\left[\sin\left(\omega_{0ia}t\right)\right]^2 dt = \\ = R_{ia}\cdot\left(I_{pki}\right)^2\cdot\frac{\left(\varphi_i-\cos\left(\varphi_i\right)\sin\left(\varphi_i\right)\right)}{2\omega_{0ia}}, \tag{5}$$

where $\omega_{0ia} = 2\pi f_{0ia}$ is the natural resonance frequency of the phase *i*, sub-state 'a'. The relationship between the peak current and the average current of phase, *i*, can be expressed as:

$$(2/\pi)\cdot I_{pki} = I_{avi}\cdot(2\cdot \mathrm{df}_i), \tag{6}$$

where $\mathrm{df}_i = f_s/f_{0i}$ is the ratio between the switching frequency and the natural frequency of the resonant network [6].

Substituting (1) and (6) into (5), and after some manipulations, the power loss of the sub-state can be expressed as a function of the average output current, I_o by:

$$P_{ia} = \left(I_o\right)^2\cdot k_i^2\frac{\pi\cdot R_{ia}}{4\cdot \mathrm{df}_i}\cdot\left(\varphi_i-\cos\left(\varphi_i\right)\sin\left(\varphi_i\right)\right). \tag{7}$$

To comply with the equivalent model (Fig. 6), the equivalent resistance of the sub-state, *i*a, is extracted from (7) to be:

$$R_{eia} = k_i^2\frac{R_{ia}\cdot\pi\cdot\varphi_i}{4\cdot \mathrm{df}_i}\left(1-\sin c\left(2\varphi_i\right)\right). \tag{8}$$

In a similar manner, all the equivalent sub-state resistances can be extracted using the steps described above. Alternatively, for the case of complementary free-wheeling action, the equivalent resistance can be derived by substituting the commutation angle φ_i, by the complementary one (π-φ_i). Naturally, for the particular case of SCP (discharging phase, i = 2), calculations are carried out with φ_i = π, that is:

$$R_{ei} = k_i^2\frac{\pi^2}{4\cdot \mathrm{df}_i}R_{ia}. \tag{9}$$

As can be observed, expression (9) extracted using the generalized approach of this study, is in agreement with the SCP modeling methodology previously reported in [6]-[9].

B. Equivalent average diode voltage source calculation

Following Fig. 5, the proportionality factor, ρ_{ia}, that represents the ratio between the charge transferred via sub-state *i*a, and the total charge via phase *i*, can be derived as follows:

$$\rho_{ia} = \frac{q_{ia}}{q_i} = \frac{I_{pkia}\int_0^{\varphi_i/\omega_{0i}}\sin\left(\omega_{0i}t\right)dt}{I_{pki}\int_0^{\pi/\omega_{0i}}\sin\left(\omega_{0i}t\right)dt} = \sin^2\left(\varphi_i/2\right). \tag{10}$$

The complementary proportionality factor in the case of two sub-states in one phase *is* $\rho_{ib} = 1 - \rho_{ia}$. In the general case of multiple phases with free-wheeling diodes, the effective average equivalent voltage drop, V_d, can be obtained by summation of (3) for all the contributing sub-states, taking into account the effect of df_i. V_d can be expressed as:

$$V_d = \sum_{i,j=1,a}^{m,n} k_i\cdot\rho_{ij}\cdot \mathrm{df}_{ij}\cdot V_{Fij}, \tag{11}$$

where *m* is the total number of switching phases, *n* is the total number of sub-states per phase *i*.

V. Simulation & Experimental (Model Validation)

To validate the proposed model, two experimental prototypes were constructed. In the first prototype, a unity gain RSCC depicted in Fig. 7 was evaluated to confirm the analytical derivation. The second experiment demonstrated strength of the modeling methodology by considering a voltage doubler RSCC configuration, as shown in Fig. 8 For both configurations, the proportionality factors were $k_{1,2}$=1, and the frequency ratio $\mathrm{df}_{1,2}$ was 1.

A. Unity Converter

The experimental setup and simulation test bench parameters were: quality factor of the resonant tank was maintained above 20, output power range was between 3 to 30 watts. Fig. 9 shows typical waveforms of the sub-state currents demonstrating DCP operation. As can be observed the phase current is commutated between two sub-states.

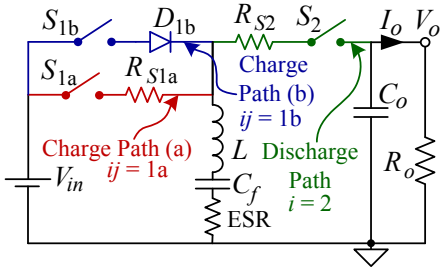

Fig. 7. Unity gain SCC switching circuit, with charge phase operated in a DCP mode. (Switch S_{1b} blocks undesired conduction paths).

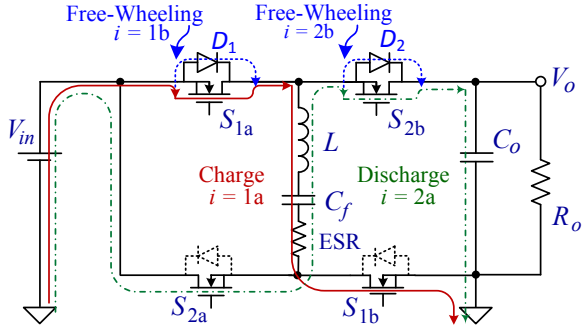

Fig. 8. Voltage doubler converter topology with free-wheeling diodes D_1, D_2. Charge: S_{1a}, S_{1b} - ON, Discharge: S_{2a}, S_{2b} - ON.

Three sets of experiments were carried out. In the first experiment, extraction of the equivalent resistance following the procedure detailed by expression (8) is verified. In this experiment the free-wheeling diode, D_{1b}, was omitted, and replaced by additional resistive conduction path using the transistor, S_{1b}, (the ratio of R_{1b} / R_{1a} was around 10) (Fig. 7). Fig. 10 shows the experimental results of the average currents at paths 1a and 1b as a function of the commutation phase φ, and the agreement to the theoretical calculations and the simulation derived results.

In the second experiment, the capability of the model to include diode losses was evaluated by implementing D_{1b} (Fig. 7) using two diodes connected in series. The total average forward voltage drop, V_F, of the two diodes at nominal current was estimated to be 1.7V. Furthermore, to emphasize the voltage drop effect, all other loss contributors were made negligibly small. Fig. 11 shows results of the average equivalent diode voltage drop, V_d, as a function of the commutation angle, φ, obtained from model calculations, simulations, and experimental measurements.

The third experiment summarizes the validity of the modeling methodology by considering both diode as well as resistive losses. This is done by changing the free-wheeling loop to include two diodes, as well as loop resistance R_{1b} (R_{1b} / R_{1a} was around 10) in a way that the loss contribution of both elements was approximately equal. Fig. 12 shows the values of the output voltage predicted by the model, simulation results and experimental measurements.

B. *Voltage Doubler SCC*

The experimental and simulation results were obtained for several values of quality factors, commutation angles, φ_i on both the charge phase (i=1) and the discharge phase (i=2), average voltage drop, V_F, and loops resistances. Also added in this experiment is a case of a voltage doubler with self-commutation (DCP mode) in both the charging and discharging phases. Figs. 13-15 show an example of the charge and discharge sub-states current waveforms, demonstrating DCP operation of the converter. The experimental parameters and comparison of the results to the one obtained from the modeling methodology are summarized in TABLE I. The model used to predict the output voltage value for this experiment is depicted in Fig. 16. A very good agreement was found between the values predicted by the model and the experimental results (approximately 1% discrepancy).

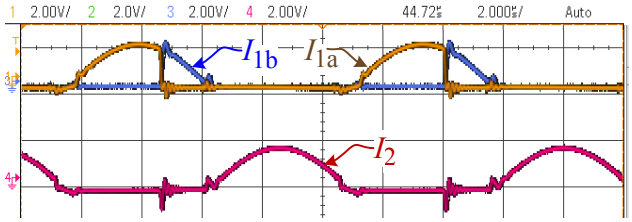

Fig. 9. Experimental waveforms obtained from a unity gain resonant SCC operating in DCP mode with $\varphi_i \approx 126°$. Upper traces – charge sub-states currents, Bottom trace – discharge current. Scale: vertical - 2A/Div, horizontal - 2µs/Div.

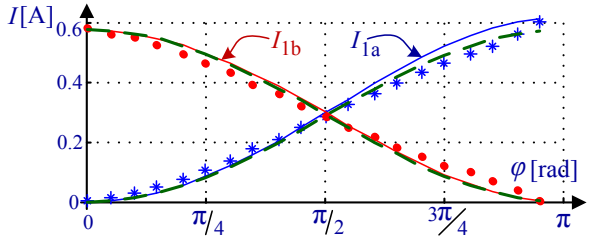

Fig. 10. Average currents at paths 1a and 1b. Model calculation - solid trace, simulation - dashed line, and experimental results – (I_{1a}) asterisk marks and (I_{1b}) circle marks.

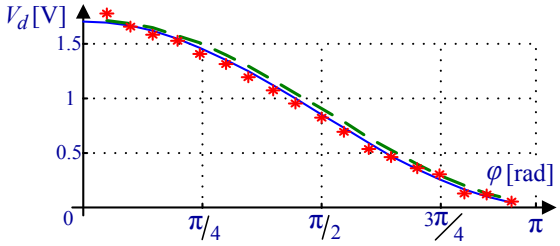

Fig. 11. Equivalent average diode voltage drop, V_d, as a function of the commutation phase, φ. Model calculation - solid trace, simulation - dashed line, and experimental results - asterisk marks.

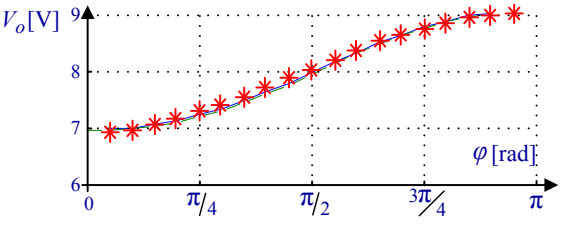

Fig. 12. Output voltage as a function of the commutation phase, φ. Model calculation - solid trace, simulation - dashed line, and experimental results - square marks.

TABLE I

Voltage doubler converter - Summary of experimental results at V_{in}=10V, C_o=100µF, f_s=35kHz.

φ_i [degrees] / Parameters	φ_1=103 φ_2=139	φ_1=149 φ_2=139	φ_1=90 φ_2=90	φ_1=90 φ_2=131	φ_1=123 φ_2=131	φ_1=150 φ_2=134	φ_1=90 φ_2=90	φ_1=139 φ_2=139
$R_{loop1a,}$ R_{loop2a} [mΩ]	100	100	370	370	370	370	700	700
$R_{loop1b,}$ R_{loop2b} [mΩ]	100	100	100	100	100	100	100	100
$Q_{1a,2a}$ (worst case)	102	102	27	27	27	27	14.6	14.6
V_F (D_1,D_2) [V]	1.7	0.85	1.7	1.7	1.7	1.7	1.7	1.7
R_o [Ω], P_o [W]	30, 11.4	50, 7.7	30, 10	30, 10.6	30, 10.9	30, 11.3	30, 9.5	30, 10.2
Efficiency	0.91	0.96	0.86	0.88	0.89	0.91	0.83	0.86
V_o (DC) Simulation [V]	18.83	19.63	17.61	18	18.31	18.54	17.14	17.65
V_o (DC) Experimental [V]	18.7	19.76	17.5	18	18.24	18.5	17	17.63
V_o (DC) Model [V]	18.79	19.65	17.62	18.18	18.36	18.46	17.12	17.67

VI. CONCLUSIONS

This paper presented a modeling approach of resonant SCC that is applicable to both the conventional resonant operation as well as for converters that operate in the more general case of a divided conduction path ZCS. The modeling concept applies representation of the resistive losses by partial equivalent resistance and losses originated from P-N junction devices, all with respect to the output current of the converter. Although exemplified on a relatively simple case of two conduction paths, the modeling methodology is well-qualified to extract the behavior of a resonant SCC with any number of split current loops.

The experimental study confirmed the validity of the modeling method to distinguish between losses types (resistive and voltage drop) with excellent agreement between the analytical derivations, simulations and experimental results. It was found that while the partial equivalent resistances are extracted as a function of the rms currents and the related commutation phase, the equivalent average diode voltage source depends primarily on the ratio between the sub-states charges (proportionality factor, ρ).

It should be noted that a self-commutation approach may not be compatible with all converter configuration. For example, converters where the voltage difference between input and output is higher than the forward voltage drop of the free-wheeling diode which may result in an undesirable current path.

The Divided Conduction Path operation mode can significantly simplify the control effort and eliminate the additional circuitry that is required to achieve zero current switching in resonant converters and in particular for resonant SCC that require active zero current detection to improve the power conversion efficiency.

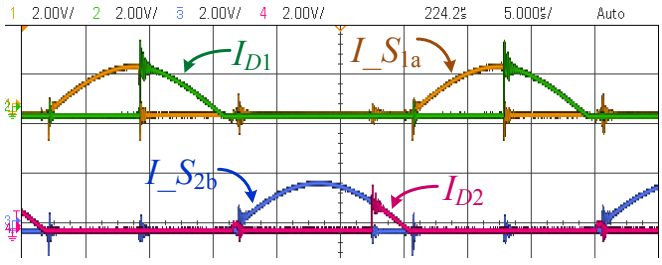

Fig. 13. Experimental waveforms obtained from a double gain resonant SCC operating in DCP mode with φ_1≈96°, φ_2≈139°, V_{in}= 10V, $R_{loop1a,2a}$=370mΩ, $R_{loop1b,2b}$=100mΩ, $V_{F1,2}$=1.7V, P_{out}=10.6W, Upper traces – charge sub-states currents, Bottom trace – discharge sub-states currents. Scale: vertical - 2A/Div, horizontal - 5µs/Div.

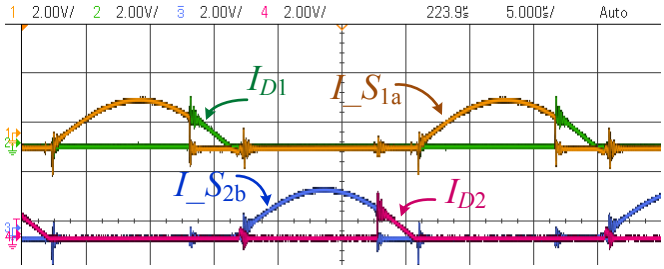

Fig. 14. Experimental waveforms obtained from a double gain resonant SCC operating in DCP mode with φ_1=φ_2≈139°, V_{in}=10V, $R_{loop1a,2a}$=370mΩ, $R_{loop1b,2b}$=100mΩ, $V_{F1,2}$=1.7V, P_{out}=11.13W. Upper traces – charge sub-states currents, Bottom trace – discharge sub-states currents. Scale: vertical - 2A/Div, horizontal - 5µs/Div.

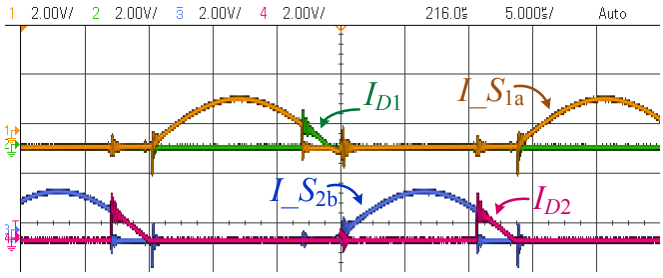

Fig. 15. Experimental waveforms obtained from a double gain resonant SCC operating in DCP mode with φ_1≈148°, φ_2≈139°, V_{in}= 10V, $R_{loop1a,2a}$=370mΩ, $R_{loop1b,2b}$=100mΩ, $V_{F1,2}$=1.7V, P_{out}=11.3W. Upper traces – charge sub-states currents, Bottom trace – discharge sub-states currents. Scale: vertical - 2A/Div, horizontal - 5µs/Div.

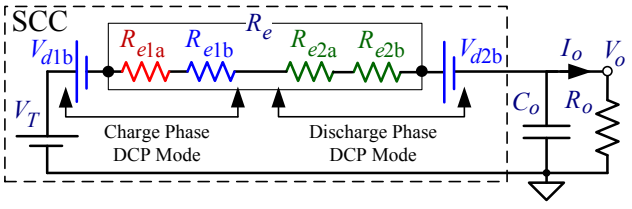

Fig. 16. SCC generic average equivalent circuit that shows the contribution of the partial sub-circuits equivalent resistances R_{ei} to the total equivalent circuit resistance R_e. (For the doubler SCC example of Fig. 8, R_{e1a} is the loss contribution of charge sub-state 1a, R_{e1b} and V_{d1b} are the resistive and diode loss contribution of the free-wheeling sub-state, respectively. R_{e2a} is the loss contribution of the discharge sub-state 2a, R_{e2b} and V_{d2b} are resistive and diode loss contribution of the free-wheeling discharge sub-state, respctively).

REFERENCES

[1] E. Hamo, A. Cervera, M.M. Peretz, "Multiple conversion ratio resonant swtiched capacitor converter with active zero current detection," *IEEE Energy Conversion Congress and Exposition, ECCE-2013,* pp.805-812 , 2013.

[2] E. Rotman and S. Ben-Yaakov, "Rapid push-pull resonant charger for high power high voltage application using low input voltage," *IEEE Energy Conversion Congress and Exposition, ECCE-2013*, pp. 2325-2332, 2013.

[3] F.T. Wakabayashi, M.J. Bonato and C.A. Canesin, "A new family of zero-current-switching PWM converter," *Power Electronics Specialists Conference, PESC-99, 30th Annual IEEE*, vol.1 pp. 451-456, 1999.

[4] Yaung-Shung Lee, Yin-Yuan Chiu and Ming-Wang Cheng, "Inverting ZCS Switched-Capacitor Bi-directional Converter," *Power Electronics Specialists Conference*, *PESC-06, 37th IEEE*, pp. 1-6, 2006.

[5] T. Mishima and M. Nakaoka, "A new family of ZCS-PWM DC-DC converters with clamping Diodes-assisted active edge-resonant cell," *International Conference on Electrical Machines and Systems, ICEMS-2010*, pp. 168-173, 2010.

[6] M. Evzelman and S. Ben-Yaakov, "Average-current-based conduction losses model of switched capacitor converters," *IEEE Trans. on Power Electronics,* vol. 28, no. 7, pp. 3341-3352, 2013.

[7] S. Ben-Yaakov and M. Evzelman, "Generic and unified model of Switched Capacitor Converters," *IEEE Energy Conversion Congress and Exposition*, *ECCE-2009*, pp. 3501-3508, 2009.

[8] S. Ben-Yaakov, "On the influence of switch resistances on switched capacitor converters losses," *IEEE Trans. on Ind. Electronics.* vol. 59, pp. 638–640, 2012.

[9] J.W. Kimball and P.T. Krein, "Analysis and Design of Switched Capacitor Converters," *IEEE Applied Power Electronics Conference and Exposition APEC-2005*, pp. 1473-1477, 2005

[10] M.Henry and J.W.Kimball, "Practical performance analysis of complex switched-capacitor converters," *IEEE Trans. on Power Electronics.*, vol. 26, no. 1, pp. 127–136, 2011.

[11] J. M. Henry and J. W. Kimball, "Switched-capacitor converter state model generator," *IEEE Trans. on Power Electronics*, vol. 27, pp.2415-2425, 2012.

[12] Jonathan W. Kimball, "Performance analysis of generalized algebraic switched Capacitor Converters," *IEEE Energy Conversion Congress and Exposition, ECCE-2013*, pp. 1808-1813, 2013.

[13] M. Shoyama and T. Ninomiya, "Output Voltage Control of Resonant Boost Switched Capacitor Converter," *IEEE Power Conversion Conference*, *PCC-07*, pp. 899-903, 2007.

[14] Y. Yuanmao, K.W.E. Cheng and Y.P.B. Yeung, "Zero-current switching switched-capacitor zero-voltage-gap automatic equalization system for series battery string," *IEEE Trans. on Power Electronics*, vol. 27, no. 7, pp. 3234-3242, 2012.

[15] I. Oota, N. Hara and F. Ueno, "Influence of parasitic inductance on serial fixed type switched-capacitor transformer," *IEEE International Symposium on Circuits and Systems, ISCAS-99*, pp. 214-217, 1999.

[16] J.W. Kimball, P.T. Krein and K.R. Cahill, "Modeling of capacitor impedance in switching converters," *IEEE Power Electronics Letters,* vol. 3, no. 4, pp. 136-140, 2005.

[17] M.S. Makowski and D. Maksimovic, "Performance Limits of Switched-Capacitor DC-DC Converters," *IEEE Power Electronics Specialists Conference*, *PESC-95*, pp. 1215-1221, 1995.

[18] M.D. Seeman and S.R. Sanders, "Analysis and optimization of switched capacitor DC-DC converters," *IEEE Trans. on Power Electronics,* vol. 23, no. 2, pp. 841-851, 2008.

[19] I. Oota, N. Hara and F. Ueno, "A general method for deriving output resistances of serial fixed type switched-capacitor power supplies," *IEEE Int. Symp*, vol. 3, pp. 503-506, 2000.